

Journal of Materials Chemistry A

Accepted Manuscript



This is an *Accepted Manuscript*, which has been through the Royal Society of Chemistry peer review process and has been accepted for publication.

Accepted Manuscripts are published online shortly after acceptance, before technical editing, formatting and proof reading. Using this free service, authors can make their results available to the community, in citable form, before we publish the edited article. We will replace this *Accepted Manuscript* with the edited and formatted *Advance Article* as soon as it is available.

You can find more information about *Accepted Manuscripts* in the [Information for Authors](#).

Please note that technical editing may introduce minor changes to the text and/or graphics, which may alter content. The journal's standard [Terms & Conditions](#) and the [Ethical guidelines](#) still apply. In no event shall the Royal Society of Chemistry be held responsible for any errors or omissions in this *Accepted Manuscript* or any consequences arising from the use of any information it contains.

Stability of $\text{NdBaCo}_{2-x}\text{Mn}_x\text{O}_{5+\delta}$ ($x = 0, 0.5$) layered perovskites in humid conditions investigated by high-temperature *in situ* neutron powder diffraction

Mona Bahout^{1*}, Stevin S. Pramana², James M. Hanlon¹, Vincent Dorcet¹, Ron Smith³, Serge Paofai¹ and Stephen J. Skinner^{2*}

¹Institut des Sciences Chimiques de Rennes, Equipe « Chimie du Solide et Matériaux », UMR CNRS 6226, Université de Rennes 1, 263 Avenue du Général Leclerc, 35042 Rennes, France

²Department of Materials, Imperial College London, Exhibition Road, London SW7 2AZ, United Kingdom

³The ISIS Facility, STFC Rutherford Appleton Laboratory, Chilton, Didcot, OX11 0QX, UK

ABSTRACT The double perovskites $\text{NdBaCo}_{2-x}\text{Mn}_x\text{O}_{5+\delta}$ ($x = 0, 0.5$) were investigated using *in situ* high temperature neutron powder diffraction in dry argon and wet atmospheres (40% D_2O /argon and 40% D_2O /air) in order to assess their stability as cathodes in proton conducting fuel cells. The $x = 0$ oxide loses oxygen on heating in dry argon at $T > 400$ °C and exhibits an oxygen vacancy order-disorder transition as evidenced by the orthorhombic $Pmmm$ to tetragonal $P4/mmm$ transition. Refinement of site occupancy factors suggest that the oxygen vacancies mainly form in the Nd layers and to lesser extent at the equatorial positions of the transition metal polyhedra; at 800 °C, $\delta \sim 0$. When the gas was changed to wet argon at 800 °C and the sample cooled to 260 °C, no structural modification or change in the oxygen content was detected and no impurity phases formed highlighting the excellent stability of the sample in wet atmosphere. On switching the gas to wet air at 260 °C, thermal analysis and neutron powder diffraction data together reveal that the sample intercalates mainly oxygen rather than proton defects within a two-phase process involving two orthorhombic phases reflecting the symmetry of the reduced and oxidised materials. On heating at $T \geq 600$ °C the sample transforms to a single tetragonal phase whose symmetry is retained up to 800 °C and on subsequent cooling. The $x = 0.5$ material prepared in argon adopted a tetragonal $P4/mmm$ structure at RT with $\delta \sim 0$. Its symmetry remains tetragonal on heating/cooling in wet argon and in wet air it uptakes oxygen at $T \sim 260$ -300 °C *via* a two-phase process involving two tetragonal phases. Since fast oxidation is the main process that fills the oxygen vacancies of these double perovskites in wet air, a large oxygen deficiency seems to be not the only requirement for effective proton incorporation in these families of materials with basic character.

Keywords: SOFC, double perovskite, *in situ* neutron diffraction, wet atmosphere, thermal analysis.

1. Introduction

Conventional solid oxide fuel cells (SOFCs) based on the oxide ion conducting electrolyte, 8 mol% yttria-stabilized zirconia (8YSZ), need high operating temperatures, between 800 and 1000 °C, to achieve sufficient ionic conductivity in the electrolyte ¹. Such high temperatures impose great challenges on the long-term stability and durability of the SOFC materials ² and require use of expensive ceramic interconnects and heat exchangers. For this reason, significant research efforts are currently devoted to reducing the operation of the SOFCs to the intermediate temperature (IT) range of ~ 400-700 °C while retaining the benefits of elevated temperatures ²⁻³. In this view, a proton conducting SOFC (H⁺-SOFC) based on a proton conducting ceramic electrolyte that can operate between 300 and 600 °C, has emerged as a promising candidate ⁴⁻⁸. Proton conduction requires the existence of proton defects in the oxide whose incorporation in the bulk oxide requires the presence of oxygen vacancies ⁸⁻⁹. Indeed, the main reaction leading to the formation of proton defects is the dissociative adsorption of water into a hydroxide ion and a proton; the hydroxide ion fills an oxide ion vacancy, and the proton forms a covalent bond with lattice oxygen ($\text{H}_2\text{O}_{(\text{gas})} + V_{\text{O}}^{\cdot\cdot} + \text{O}_{\text{O}}^{\text{x}} \leftrightarrow 2\text{OH}_{\text{O}}^{\cdot}$ in the Kröger-Vink notation). Proton conduction consists of the hopping of protons between neighboring oxygen positions, termed as the Grotthuss (or free-proton) mechanism.

Besides the search for suitable electrolytes combining high proton conductivity at moderate temperature with thermodynamic stability, the development of cathode materials for H⁺-SOFC with fast transfer kinetics in the *IT* range is another challenging issue ¹⁰. The cathode plays a critical role in proton conducting fuel cells because water is produced at the cathode. Most work on H⁺-SOFC has been carried out using Pt electrodes surrounding doped cerate (ACeO₃) or zirconate (AZrO₃) proton conducting electrolytes. Despite their good catalytic activity, Pt electrodes exhibit large overpotential and are too expensive for large-scale applications ¹¹. Recently, double-layered perovskite oxides,

$LnBaCo_2O_{5+\delta}$ have been investigated as the cathode in H^+ -SOFC^{10, 12-13}. The Co-based layered double perovskite oxides, $LnBaCo_2O_{5+\delta}$ ($Ln = La, Pr, Nd, Sm, Gd, \text{ and } Y$)¹⁴ were extensively investigated as cathode materials for O^{2-} -SOFCs due to their excellent electrochemical properties correlated to their mixed conductivity (O^{2-}/e^-)¹⁵⁻¹⁶. Their structure consists of A -site ordering into alternate layers of Ln and Ba ions with oxygen vacancies primarily located in the LnO_δ layers. A variety of unit cells were reported for $LnBaCo_2O_{5+\delta}$ compounds at various temperatures and δ ranges; the most common are $P4/mmm$ ($a_p \times a_p \times 2a_p$) and $Pmmm$ ($a_p \times 2a_p \times 2a_p$), where a_p is the lattice parameter of a simple cubic perovskite. The behaviour of $LnBaCo_2O_{5+\delta}$ compounds in wet air was previously investigated by thermogravimetric analysis (TGA) and chemical compatibility tests with the $BaZr_{0.9}Y_{0.1}O_{3-\delta}$ proton conducting electrolyte revealed no impurity phases¹². The oxygen reduction reaction was investigated by electrochemical impedance spectroscopy as a function of water vapor pressure, p_{H_2O} , and demonstrated improved performance with increased p_{H_2O} which was attributed to insertion of protonic defects (OH_o^\cdot) into the structure¹³. Although such behaviour may indicate protonic conductivity in the $LnBaCo_2O_{5+\delta}$ materials, this needs to be established unambiguously, since there is no direct evidence of the presence of structural protons in this family of materials. Due to the sensitivity of neutron diffraction to both the light atom positions and site occupancies, we undertook an *in situ* high temperature study in dry and wet (D_2O) argon; and wet (D_2O) air on two double perovskite compounds, $NdBaCo_{2-x}Mn_xO_{5-\delta}$ ($x = 0$ and 0.5), using time-of-flight (TOF) neutron powder diffraction (NPD). The aim was to verify their stability and monitor their structural behaviour under operating conditions relevant to H^+ -SOFC cathodes. Since insertion of proton defects in typical proton conducting electrolytes occurs between 300 and 600 °C and dehydration/deprotonation prevails at higher temperatures⁷, isothermal neutron diffraction data were collected in the temperature range 260-800 °C. The $x = 0.5$ and $x = 0$ compositions have been investigated in order to shed light on the impact of the electronegativity of the B cation as well as that of crystal symmetry and oxygen content on the hydration capacity and stability in wet conditions. It is well known that in perovskite type proton conducting electrolytes, the electronegativity of the B cation impacts the stabilization of proton defects and any symmetry reduction reduces water

solubility⁷. In contrast to the $x = 0$ composition whose symmetry changes between orthorhombic and tetragonal as a function of temperature and gas atmosphere, the symmetry of the $x = 0.5$ material is tetragonal and remains unchanged on heating/cooling in air or in inert atmosphere¹⁷.

Experimental

The preparation of the polycrystalline samples ($x = 0, 0.5$) has been described elsewhere¹⁸. Phase purity was assessed by powder X-ray diffraction (XRD) collected at room temperature over the range $10 \leq 2\theta \leq 120^\circ$, $\Delta 2\theta = 0.02^\circ$ using a Bruker AXS D8 Advance diffractometer in Bragg-Brentano geometry equipped with Ge primary monochromator (Cu-K α_1 radiation) and a Lynxeye detector. Initial oxygen content was determined *via* iodometric titration against a standardized sodium thiosulfate solution (~ 0.05 M). A powder sample (~ 300 mg) was introduced in a closed argon-flushed glass container and covered by a large excess of KI (~ 2 g). Approximately 20 mL of hydrochloric acid twice diluted was added to the warm mixture ($\sim 40^\circ\text{C}$) that was stirred under an argon flow. When dissolution was complete, the iodine formed was titrated under argon flow with Na₂S₂O₃ solution and the calculated oxygen stoichiometry was based on the amount of I₂ formed. Thermogravimetric analysis (TGA) was carried out using a Netzsch STA 449 F3 instrument. Samples weighing ~ 100 mg, loaded in platinum crucibles, were heated to 800 °C at a rate of 10 °C min⁻¹ in 1 atm of dry air (40 mL min⁻¹) before cooling in air at 10 °C min⁻¹. This cycle was performed to clean the sample from absorbed free water, hydrates, hydroxides and carbonates. Subsequent cycles were carried out in dry gas and in dry + wet gas, as detailed in the *Results and Discussion*.

In situ neutron diffraction data were collected on the high-flux medium resolution POLARIS diffractometer at ISIS, the UK spallation source at the Rutherford Appleton Laboratory. The powder samples were loaded into a quartz cell up to a height of a 4 cm to ensure maximum material was exposed to the beam in a flow-through mode, allowing switching between gas streams (e.g. dry and wet). The temperature ramp was always 10 °C min⁻¹. Two thermocouples were attached on opposite sides of the outer wall of the quartz ampoule and just above the neutron beam (i.e. sample) to control

and monitor the furnace temperature respectively. The samples were first heated from 20 to 800 °C in dry argon to clean the surface area from protonic species ($\text{Ba}(\text{OH})_2$, $\text{Ba}(\text{OH})_2 \cdot n\text{H}_2\text{O}$, $\text{Ba}(\text{OH})_x(\text{CO}_3)_y \cdot n\text{H}_2\text{O}$) and to increase the amount of oxygen vacancies which may favour the insertion of proton defects. Subsequently, the atmosphere was changed to wet argon. The humid atmosphere was generated with D_2O in preference to H_2O (the coherent scattering lengths of H and D are -3.7406 and 6.671 fm, respectively). In addition the incoherent scattering cross section of D (2.05 barn) is much lower than H (80.27 barn)¹⁹. The D_2O injector was connected to the cell and the humidifier was set at 60 °C to provide a saturated vapor pressure roughly 0.2 bar at atmospheric pressure. Neutron diffraction data were collected on the $x = 0$ and 0.5 samples according to the profiles illustrated in Figure 1 which were chosen to complement the TGA data.

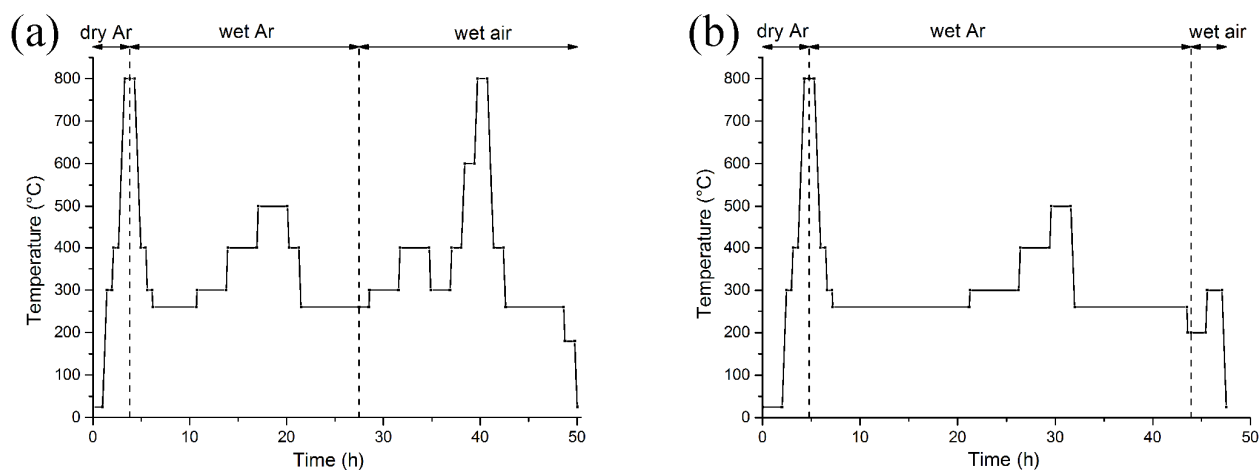


Figure 1. Temperature profile for (a) $\text{NdBaCo}_2\text{O}_{5+\delta}$ and (b) $\text{NdBaCo}_{1.5}\text{Mn}_{0.5}\text{O}_{5+\delta}$.

The main difference in the temperature profiles used for the two compositions lies in more numerous data collected in wet air on $x = 0$ than on $x = 0.5$. Since the former composition exhibits various phase transitions, we investigated any changes in symmetry/crystal structure, oxygen content or hydroxyl intercalation/deintercalation, stability in wet air, kinetics of oxygen exchange and thermodynamic equilibrium as a function of temperature. Data normalisation and file output was done using the Mantid software package²⁰. The patterns from two banks of detectors; the new backscattering bank ($2\theta = 146.7^\circ$) which covers a range in 2θ from 135 to 167° with a d -spacing range of 0.2 - 2.65 Å and the new

90° bank ($2\theta = 92.6^\circ$) which covers a 2θ range of 75 to 113° with a maximum d -spacing of 4.1 Å were simultaneously fitted by the Rietveld method using the FullProf refinement program²¹. Peak shapes were modeled using a convolution of two back-to-back exponentials with a pseudo-Voigt function. The background due to the amorphous quartz cell was estimated from linear interpolation between manually selected N points ($40 \leq N \leq 70$) and they were ensured not to interact with the Bragg reflections of the phase of interest. In addition to the profile parameter (σ_1) describing the Gaussian contribution to the Bragg peak profiles, anisotropic strain broadening parameters (i.e. hkl dependent) have been refined through the S_{HKL} microstrain parameters in Stephen's model²². The lattice parameters, fractional occupancy of all oxygen sites, atomic positions and atomic displacement parameters (either isotropic or anisotropic) were refined for each pattern. Any additional constraints are noted when describing specific models. Electron diffraction (ED) experiments at room temperature were performed using a Transmission Electron Microscope (TEM) JEOL2100 LaB₆ operating at 200 kV. Powders of $x = 0, 0.5$ were crushed in dry ethanol and a drop of the suspension was deposited on a copper grid covered by a carbon film. Diffractions patterns were collected with a GATAN Orius 200D Charge Coupled Device (CCD) Camera.

Results and discussion

3.1 Thermogravimetric analysis

The behaviour of the $x = 0$ and 0.5 compositions was studied by thermogravimetric analysis in wet air ($p_{\text{H}_2\text{O}} = 0.18\text{-}0.60$ atm) to check the influence of the presence of oxygen vacancies on water uptake in these electronic conducting phases. Two series of measurements were collected according to the following procedure: the powders were heated in dry N₂ from RT up to 800 °C at a rate of 10 °C min⁻¹ followed by isothermal heating at 800 °C for 1 h, in order to achieve thermodynamic equilibrium and maximize the oxygen vacancy content. The sample was then cooled to 260 °C at a rate of 10 °C min⁻¹ in dry N₂ and held at 260 °C for 1 h. Afterwards, the gas was changed to dry air and after equilibration the sample was stepwise heated to 800 °C before cooling. To check for possible water insertion, a second

treatment consisted of heating the powder in wet air up to 800 °C after the heating/cooling cycle performed in dry N₂. Thermogravimetric data measured for the $x = 0$ sample are displayed in Fig. 2.

The large mass decrease subsequent to the heating/cooling cycle in dry nitrogen ($\Delta m/m \sim 1.75\%$) corresponding to loss of ~ 0.5 oxygen/f.u. suggests the formation of a large number of oxygen vacancies. As soon as the gas was changed to dry air at 260 °C, a sharp mass increase immediately occurred reflecting fast oxygen exchange and suggesting that the sample recovered its initial oxygen composition (NdBaCo₂O_{5.5}). On heating at $T > 260$ °C, the mass decreased reflecting fast reversible oxygen exchange with the atmosphere.

Switching to wet air after the heating/cooling cycle performed in dry N₂, induces an instantaneous mass increase similar to that observed in dry air. After the stepwise heating to 800 °C and subsequent cooling, a small difference in weight (0.6%) with respect to cycling in dry air was observed. The mass of the $x = 0.5$ sample exhibits little change in dry N₂ reflecting the stability of this composition towards oxygen and humidity when stored in ambient conditions. When heated in air at 260 °C, the behaviour is similar to that of the $x = 0$ sample reflecting immediate chemical oxidation and possible reversible insertion of proton defects (Figure S.I. 1).

It is important to stress that the difference in mass between the ‘wet’ and ‘dry’ treatments observed for the $x = 0$ and 0.5 samples may indicate the intercalation of proton defects and also reveal adsorption of free molecules of water and protonic entities such as hydroxide or carbonate. For example, in the XRD of the PrBaCo₂O_{5+ δ} sample hydrated at 500 °C for 12h in wet air ($p_{\text{H}_2\text{O}} \sim 0.1$ bar), Grimaud *et al.* showed evidence of formation of barium carbonate¹³. Since oxidation is the main process that fills the oxygen vacancies of highly deficient double perovskites in wet and dry air, a large oxygen deficiency seems to be not the only requirement for effective proton incorporation in the LnBaCo₂O_{5+ δ} family of materials, likely due to a limiting number of lowest energy sites for the protons in this *A*-site ordered double perovskite layered structure. Indeed, whereas water solubility approaches the saturation limit in cubic perovskite-type proton conducting electrolytes such as SrTi_{0.95}Sc_{0.05}O_{3- δ} ²³, water solubility is reduced in distorted perovskite-type electrolytes and complex perovskites which may exhibit *B*-site

ordering²³⁻²⁴. To check the stability of the layered perovskites, $\text{NdBaCo}_{2-x}\text{Mn}_x\text{O}_{5+\delta}$, $x = 0$ and 0.5 in humid conditions, diffraction experiments have been undertaken

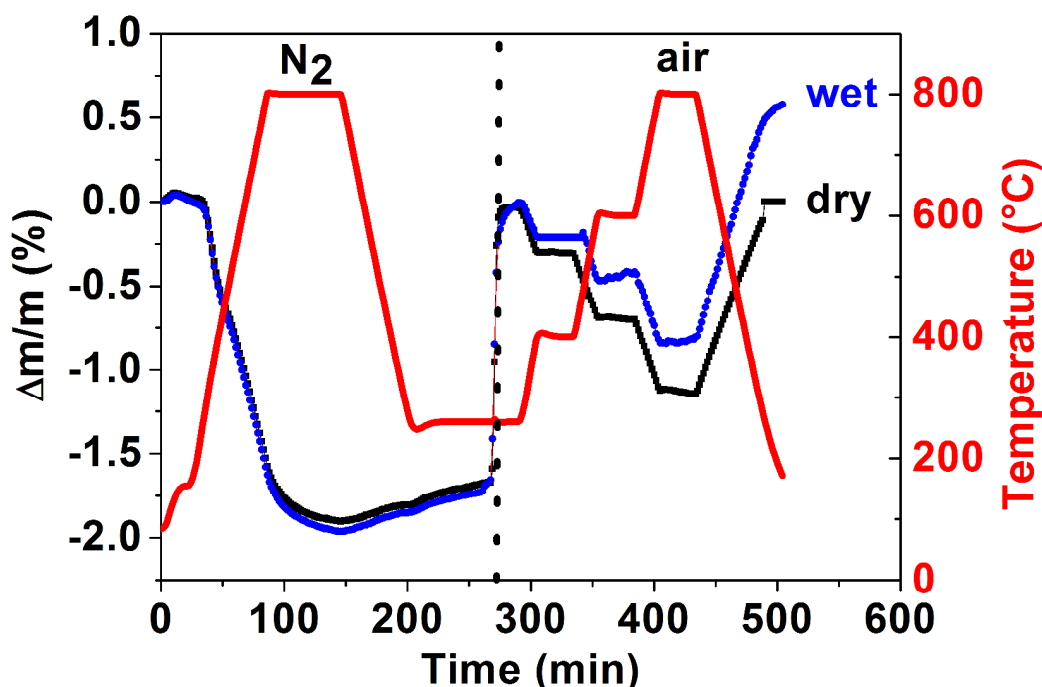


Figure 2. Thermogravimetric Analysis (TGA) of $\text{NdBaCo}_{2-x}\text{O}_{5+\delta}$ in dry N_2 and subsequent heating/cooling cycles in dry (cycle 1) and wet air (cycle 2); heating/cooling rate is $10\text{ }^\circ\text{Cmin}^{-1}$ and flow rate is 100 mL/min . Gas change from N_2 to air at $260\text{ }^\circ\text{C}$ is indicated by a vertical dot line.

3.2 Structural analysis at room temperature

3.2.1 X-ray diffraction of dry and hydrated $x = 0$ and $x = 0.5$ samples

The powders of the $x = 0$ and $x = 0.5$ samples were heated under dry air at from $20\text{ }^\circ\text{C}$ to $800\text{ }^\circ\text{C}$ at $1\text{ }^\circ\text{C min}^{-1}$ and held at $800\text{ }^\circ\text{C}$ for 1 h before cooling ($1\text{ }^\circ\text{C min}^{-1}$) to $20\text{ }^\circ\text{C}$ to obtain ‘dry’ samples. The same thermal profile was carried out in wet air ($p_{\text{H}_2\text{O}} \sim 0.6\text{ bar}$) to obtain ‘wet’ samples. Both dry and wet samples were confirmed to be single phase by X-ray powder diffraction. The structure of the ‘wet’ $x = 0$ sample was found to be orthorhombic with the space group $Pmmm$ with unit cell data, $a = 3.89048(1)$, $b = 3.90430(1)$, $c = 7.61791(2)\text{ \AA}$ and $V = 115.720(1)\text{ \AA}^3$. The quality of the refinement for the “dry” and “wet” samples was similar, $\chi^2 \sim 1.8$ and ~ 1.6 , respectively. The symmetry of the ‘wet’ and ‘dry’ $x = 0.5$ samples were found to be tetragonal with the space group $P4/mmm$; the unit cell data for the wet sample are $a = 3.89691(2)$, $c = 7.65564(4)\text{ \AA}$ and $V = 116.258(2)\text{ \AA}^3$. No major modification appears in wet air

in comparison to heating in dry air except a slight increase and decrease in the a and c lattice parameters, respectively. After heating in wet air, the unit cell volumes of the $x = 0$ and 0.5 samples exhibit a small expansion ($\Delta V/V \sim 0.1\%$) with respect to the volume obtained after heating in dry air. The XRD patterns recorded at RT for the $x = 0$ and 0.5 ‘wet’ samples are displayed in Figure S.I. 2, as supporting information.

3.2.2 Electron diffraction

Selected Area Electron Diffraction (SAED) patterns for $x = 0$ and $x = 0.5$ are presented in Figure 3 for the $[100]$ Zone Axis. The patterns were indexed according to the pseudo cubic unit cell of the perovskite structure.

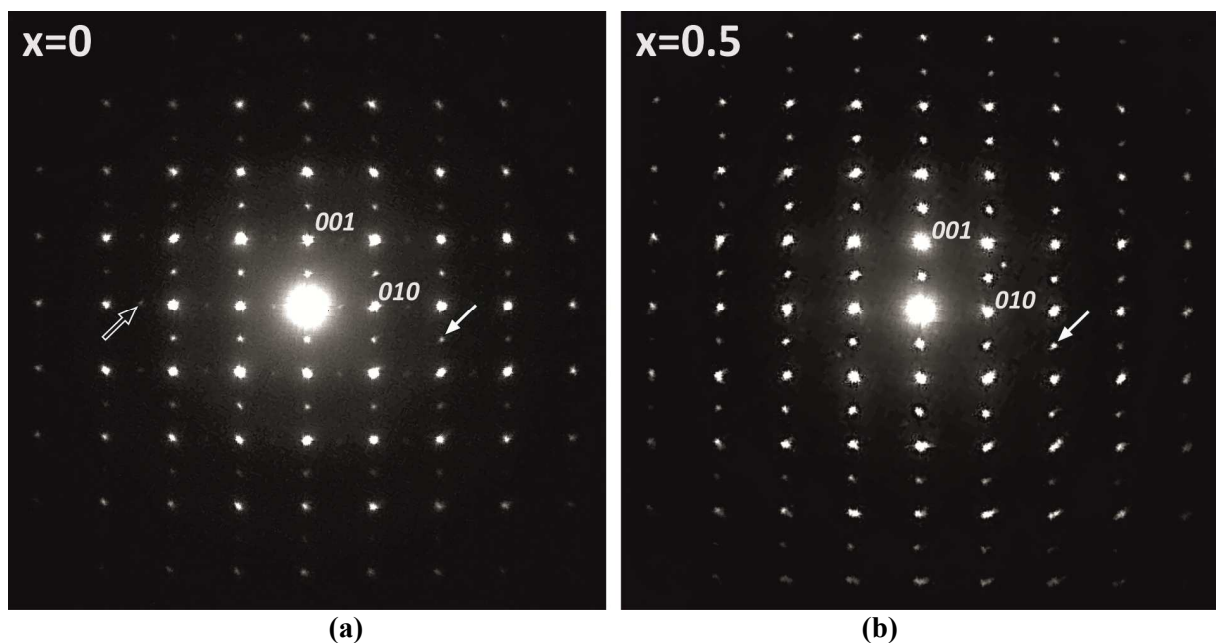


Figure 3. $[100]$ zone axis electron diffraction patterns of (a) $\text{NdBaCo}_2\text{O}_{5+\delta}$ ($x = 0$) and (b) $\text{NdBaCo}_{1.5}\text{Mn}_{0.5}\text{O}_{5+\delta}$ ($x = 1.5$). The patterns are indexed considering the cubic parent perovskite unit cell. The white arrows in $x = 0$ and $x = 0.5$ indicate superstructure reflections related to A -site cation ordering along the c -axis whereas the black arrow in $x = 0$ indicates a superstructure reflection resulting in cell doubling in b due to oxygen vacancies ordering.

SAED revealed the existence of two main structural features for the $x = 0$ composition: doubling of two lattice parameter corresponding to an $a_p \times 2a_p \times 2a_p$ supercell where a_p is the lattice parameter for the cubic perovskite was observed. The superstructure reflections along c^* have stronger intensities than those along b^* in agreement with ordering of the Nd and Ba cations in alternate layers along the c -axis

and ordering between oxygen and vacancies along the b -axis in the lanthanide layer, as reported in the literature¹⁴. For the $x = 0.5$ composition (Figure 3b), the cation ordering between Nd and Ba cations is retained whereas oxygen and vacancy ordering along b^* has disappeared likely due to lower oxygen content due to synthesis under reduced oxygen pressure (i.e. argon atmosphere)¹⁸.

3.2.3 Neutron diffraction as a function of temperature and gas atmosphere

$NdBaCo_2O_{5+\delta}$ ($x = 0$)

The room temperature (RT) Rietveld fit of the neutron powder diffraction (NPD) data for the as-prepared $NdBaCo_2O_{5+\delta}$ ($x = 0$) is displayed in Figure 4. The pattern can be indexed using $a_p \times 2a_p \times 2a_p$ unit cell (space group $Pmmm$) as determined by SAED. The doublet at $d \sim 1.95$ Å indexed as 200/040 is consistent with the orthorhombic symmetry and the superstructure low intensity peaks (e.g. 014 at $d \sim 1.84$ Å) are associated with ordering of the oxygen vacancies which occurs when the δ value is close to 0.5.

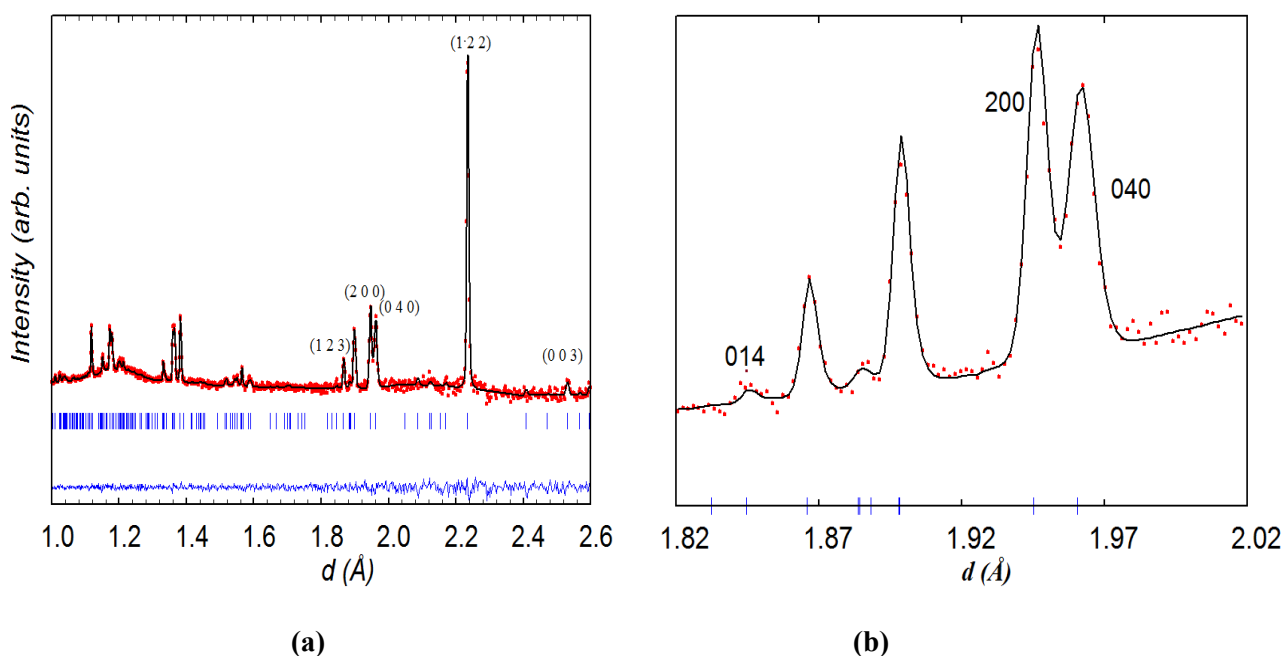


Figure 4. (a) Rietveld refinement at room temperature from the backscattering bank of $NdBaCo_2O_{5+\delta}$, with (b) an emphasis on $1.82 < d < 2.02$ Å showing the superstructure peak of 014 associated with the ordering of the oxygen vacancies. Indexing refers to the $(a \times 2a_p \times 2a_p)$ cell.

The orthorhombic crystal structure $a_p \times 2a_p \times 2a_p$ comprises two crystallographically distinct cobalt sites; Co1 and Co2 in octahedral and pyramidal coordination respectively and seven crystallographically

independent oxygen atoms; O1 and O2 in the Ba layer, O3, O4 and O5 at the equatorial positions of the Co polyhedra, O6 and O7 in the Nd layer (Figure 5).

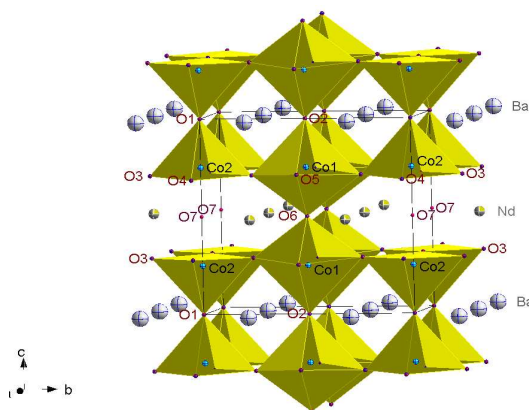


Figure 5. Crystal structure of NdBaCo₂O_{5.5} highlighting the seven crystallographically distinct oxygen positions. Ordering of oxygen vacancies was observed in the Nd layer, with O6 preferentially occupied and O7 partially unoccupied.

The atomic displacement parameters (ADP) of all the atoms were refined isotropically. Due to high correlations with site occupancy, the ADPs of the oxygen atoms in the same layer were initially constrained to be equal. However, this gave very small values for B_{iso} of the oxygen atoms in the Nd layer (O6 and O7) in comparison to the B_{iso} of the other oxygen atoms. Consequently, the B_{iso} of all the oxygen atoms were constrained to be equal. Refinement of site occupancies showed that the oxygen vacancies were primarily on one of the two crystallographically independent oxygen sites located in the Nd layers and may exist at the nearest-neighbor O3, O4 and O5 sites in the Co-layer. The difference in site occupancy between O6 [1.00(5)] and O7 [0.20(4)] is consistent with vacancy ordering²⁵⁻²⁶. The occupancy factors of the oxygen sites in the Ba layer (O1 and O2) are within a standard deviation of 1.0 and were therefore fixed to 1.0. Moreover this value did not vary when the sample was heated/cooled in Ar or air and was therefore maintained fixed in all of the refinements. The total oxygen content corresponded to 5.5(2) atoms/formula unit (f.u.) and agreed with iodometric titration results¹⁸. Therefore, mainly Co³⁺ ions are present in octahedral CoO₆ and pyramidal CoO₅ environments. The structural parameters of NdBaCo₂O_{5+ δ} at *RT* are listed in Table 1.

Table 1. Structural results from Rietveld analysis of neutron powder diffraction data for NdBaCo₂O_{5+δ} at room temperature.

Atom	Position (z) Occupation factor (Occ.)	B_{iso} (Å ²)
Nd	y: 0.271(1)	0.74(8)
Ba	y: 0.250(1)	0.7(1)
Co1	z: 0.247(2)	0.7(2)
Co2	z: 0.255(2)	0.3(2)
O1, O2	Occ : *1.00	#1.14(5)
O3	y : 0.2393(1) z: 0.2868(1) Occ : 0.98(2)	#1.14(5)
O4	z : 0.306(2) Occ : 0.94(4)	#1.14(5)
O5	z : 0.268(2) Occ : 0.98(4)	#1.14(5)
O6	Occ : 1.00(5)	#1.14(5)
O7	Occ: 0.20(4)	#1.14(5)
O-content	5.5(2)	

Space group *Pmmm*, $a = 3.8914(2)$ Å, $b = 7.84422(44)$ Å, $c = 7.59312(42)$ Å with sites Nd 2p (0.5 y 0.5), Ba 2o (0.5 y 0), Co1 2r (0 0.5 z), Co2 2q (0 0 z), O1 1a (0 0 0), O2 1e (0 0.5 0), O3 4u (0 y z), O4 2s (0.5 0 z), O5 2t (0.5 0.5 z), O6 1g (0 0.5 0.5), O7 1c (0 0 0.5); #: constrained, *: fixed, $\chi^2 \sim 0.9$, $R_B \sim 2.8\%$, $R_F \sim 2.8\%$.

In contrast to NdBaCo₂O_{5+δ}, the symmetry of NdBaCo_{1.5}Mn_{0.5}O_{5+δ} ($x = 0.5$) at room temperature was found to be tetragonal *P4/mmm* with unit cell $a_p \times a_p \times 2a_p$. This model has a single transition metal site for the (Co/Mn) ions and three O sites (O1, O2 and O3). The crystal structure and the Rietveld plot at room temperature are visualized in Figure 6. Excluded region at $1.49 < d < 1.51$ Å was introduced for a small bump likely due to an experimental artifact. The mixed B-site possesses weak overall scattering due to the competing Mn and Co scattering lengths, -3.73 and 2.49 fm, respectively. When the ADPs of

the mixed site were refined anisotropically, this appeared to cause slightly negative β_{33} for (Co,Mn) and large standard deviations for O1 whose occupancy was very low. Therefore the ADP of (Co/Mn) was refined isotropically and the B_{iso} of O1 was fixed at 0. Refinement results indicated that the majority of vacancies were contained in the Nd layer at the O1 site whose occupancy refined to $\sim 0.088(8)$, none at the O2 site whose occupancy factor was therefore fixed at 1.0 and very little at the O3 site. The overall oxygen content of $\sim 5.00(8)/\text{f.u.}$ corresponds to an equal amount of $(\text{Co,Mn})^{3+}$ and $(\text{Co,Mn})^{2+}$ cations in a square pyramidal coordination. The change from orthorhombic to tetragonal symmetry between the $x = 0$ and $x = 0.5$ compositions and the absence of the superstructure reflections related to vacancy ordering in the latter are consistent with the SAED pattern. The higher symmetry of the $x = 0.5$ compound is due to the presence of a very small amount of oxygen atoms in the Nd-layer due to the annealing conditions in the inert atmosphere required to prevent the stabilization of the hexagonal perovskite $\text{BaMnO}_{3-\delta}$ impurity¹⁸. The R factors and refined structural parameters for $x = 0.5$ at RT are given in Table 2.

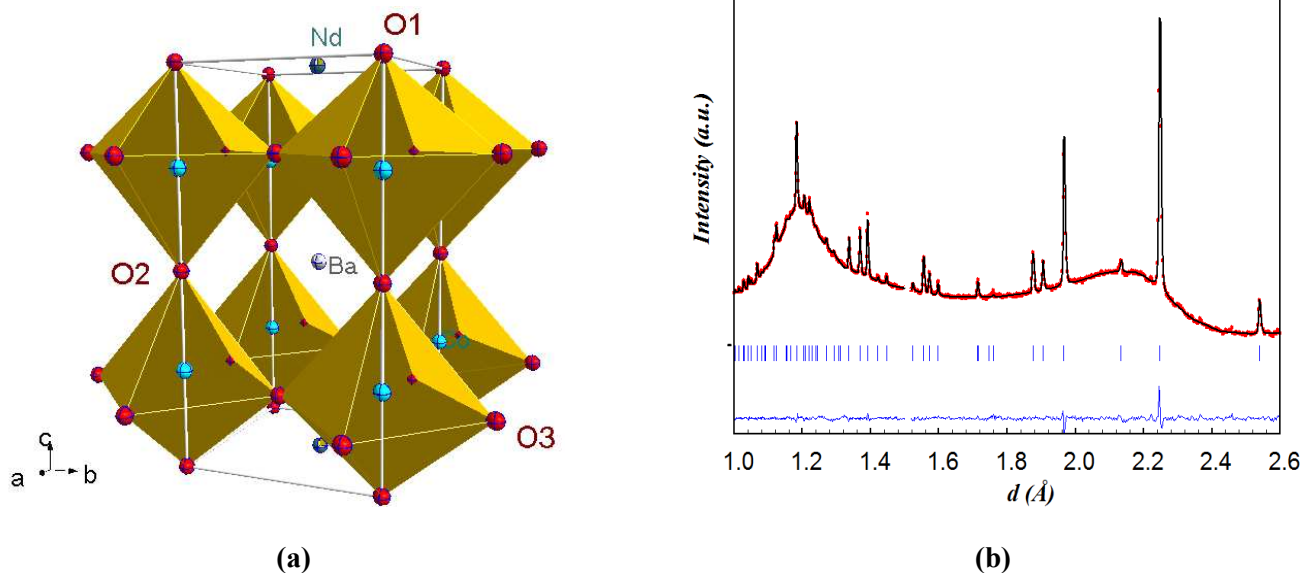


Figure 6. (a) Crystal structure of $\text{NdBaCo}_{0.5}\text{Mn}_{0.5}\text{O}_{5+\delta}$ ($P4/mmm$) with the transition metals highlighted in blue (b) Rietveld refinement at room temperature from the backscattering data bank. The undulating background is due to the quartz sample environment. Excluded region at $1.49 < d < 1.51 \text{ \AA}$ was introduced for a small bump likely due to an experimental artifact.

Table 2. Structural results obtained from Rietveld fit of neutron powder diffraction data for NdBaCo_{1.5}Mn_{0.5}O_{5+δ} at room temperature

Atom	Position (z) Occupation factor (Occ.)	$\beta_{11}, \beta_{22}, \beta_{33}$ ($\times 100$)
Nd		1.4(1), 1.4(1), 0.20(6)
Ba		1.3(2), 1.3(2), 0.6(1)
Co,Mn	$z: 0.251(2)$	*0.7(2)
O1	Occ: 0.088(8)	0.0
O2	[#] Occ: 1.0	1.5(2), 1.5(2), 0.25(8)
O3	$z: 0.1981(2)$ Occ: 0.98(2)	1.6(2), 2.4(2), 0.44(5)
O content	5.00(8)	

Space group $P4/mmm$, $a = 3.9334(1)$ Å, $c = 7.6197(4)$ Å with sites Nd $1a$ (0 0 0), Ba $1b$ (0 0 0.5), Co $2h$ (0.5 0.5 z), O1 $1c$ (0.5 0.5 0), O2 $1d$ (0.5 0.5 0.5), O3 $4i$ (0.5 0 z), [#]fixed, * refined isotropically, $\chi^2 \sim 2.1$, $R_B \sim 2.2\%$, $R_F \sim 3.0\%$.

3.3 Structural analysis as a function of temperature in an argon atmosphere

3.3.1 NdBaCo₂O_{5+δ}

The NdBaCo₂O_{5+δ} sample was stepwise heated in dry Ar up to 800 °C before switching to wet gas. This heating was performed to dry the sample and maximize the oxygen-ion vacancy content in the lattice as it may favor incorporation of proton defects. Indeed, for some Ruddlesden-Popper (RP) phases such as Sr₃FeMnO_{7-δ}, increasing the amount of oxygen vacancies by annealing in N₂ atmosphere at 500 °C was shown to have a positive impact on the hydration reaction, possibly due to kinetics²⁷. In the analysis of the data collected above room temperature in argon atmosphere, isotropic ADPs were refined for all the atoms and for all the oxygen atoms they were constrained to be the same. Isothermal data sets collected for 30 minutes at 300 and 400 °C show insignificant variations in oxygen content along with retention of the orthorhombic space group. This agrees with the TGA carried out in N₂ atmosphere which indicates mass loss above $T \sim 400$ °C (Figure 2). At 800 °C, the structure has transformed to tetragonal (S.G. $P4/mmm$); the doublet (040, 200) merged into a single peak and the small peaks associated with

oxygen-vacancy ordering have disappeared. The tetragonal structural model used in the refinements of the data collected at 800 °C and on subsequent cooling in wet argon is the same as that used for the $x = 0.5$ composition, illustrated in Figure 6a. Note that for all the rare-earth double perovskites, heating accompanied by decreasing of the oxygen content from 6 to 5 causes a series of structural transformations in the sequence “tetragonal-orthorhombic-tetragonal”. For $\text{NdBaCo}_2\text{O}_{5+\delta}$, the orthorhombic to tetragonal transition was reported to occur at $T \sim 500$ °C according to *in situ* X-ray diffraction in air²⁸. The oxygen occupancy remained unchanged in the Ba layer at temperatures of up to 800 °C whereas it decreased in the Nd layers and at the equatorial positions of the Co polyhedra; at 800 °C the occupancy of O1 and O3 sites refined to 0.42(5) and 0.88(3), respectively and the overall oxygen content of $\sim 5.0(1)$ atoms/f.u. is in good agreement with the value of 5.14(2) measured by Cox-Galhotra *et al.* in similar conditions ($T = 777$ °C , $p\text{O}_2 = 10^{-4}$ atm)²⁹ and with the value reached after the TGA cycle performed in N_2 atmosphere (Figure 2). At 800 °C, the gas was switched to wet (40%D₂O/Ar) and the same structural model was used for the dry and hydrated samples. Rietveld analysis of the data set collected at 800 °C for 30 minutes in wet argon indicated a possible slight decrease in the occupancy of O1 to $\sim 0.32(2)$ due to incomplete equilibration on holding the sample for 30 minutes at 800°C in dry Ar. Conversely, the occupancy of O3 $\sim 0.90(3)$ remains unchanged within the esd's; the overall oxygen content corresponds to 4.9(1) atoms/f.u. Neither structure distortion nor significant change in the cell parameters between data collected in both dry and wet argon at 800 °C was observed; the same thermodynamic equilibrium appears to be reached on heating in each atmosphere within 30 minutes. Moreover, no additional peaks related to sample decomposition were observed, highlighting the excellent stability of $\text{NdBaCo}_2\text{O}_{5+\delta}$ in humid conditions in contrast to the double perovskite $\text{Ba}_3\text{Ca}_{1.18}\text{Nb}_{1.82}\text{O}_{9-\delta}$ (BCN18) where the presence of secondary phases, mostly hydroxides was evidenced³⁰⁻³¹. However, it should be mentioned that if impurities are limited to traces levels their detection is difficult in diffraction experiments. A Rietveld profile from data recorded at 800 °C in wet argon is shown in Figure 7 and the relevant structural parameters derived for both dry and wet atmospheres are displayed in Table 3.

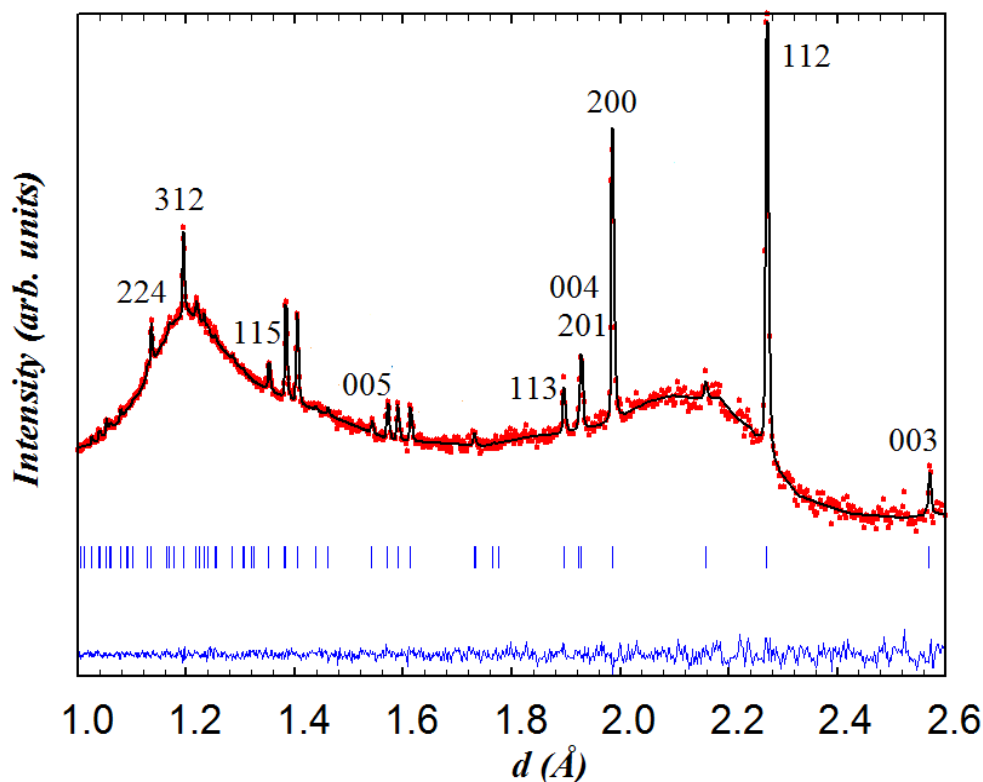


Figure 7. Rietveld refinement for $\text{NdBaCo}_2\text{O}_{5+\delta}$ recorded *in-situ* at 800 °C under wet argon; data collected for 30 min from backscattering detector bank. The indexing refers to the $(a \times a_p \times 2a_p)$ cell. The undulating background is due to the quartz sample environment.

Table 3. Rietveld parameters in dry and wet argon at 800 °C for $\text{NdBaCo}_2\text{O}_{5+\delta}$ ($P4/mmm$) with sites Nd 1a (0 0 0), Ba 1b (0 0 0.5), Co 2h (0.5 0.5 z), O1 1c (0.5 0.5 0), O2 1d (0.5 0.5 0.5), O3 4i (0.5 0 z). The ADPs of the metals were refined anisotropically, B_{iso} for the oxygen atoms were constrained to be the same.

$\text{NdBaCo}_2\text{O}_{5+\delta}$	Dry Ar, 800 °C	Wet Ar, 800 °C
a (Å)	3.9657(3)	3.9712(4)
c (Å)	7.7179(8)	7.7117(9)
Co (z)	0.246(3)	0.249(2)
O3(z)	0.2091(7)	0.2063(6)
Occ. O1	0.42(3)	0.32(2)

Occ. O3	0.88(3)	0.90(3)
O-content	5.0(1)	4.9(1)
χ^2	0.65	0.7
$R_B\%$	4.2	3.7
$R_F\%$	10.8	11.3

The sample was therefore stepwise cooled in wet argon meanwhile data sets were collected at different temperatures to allow possible hydration/dehydration to be monitored through the variation of the oxygen content. Rietveld analysis of the data sets collected at relevant temperatures and performed using anisotropic ADPs for the metal positions and isotropic ADPs for the oxygen sites (since anisotropic ADPs gave negative value of β_{33} for (O1)) did not show significant variation in the oxygen occupancy. Figure 8 shows the Rietveld fit of the pattern collected at 260 °C, the lowest temperature reached on cooling in wet argon. Relevant structural parameters are given in Table 4.

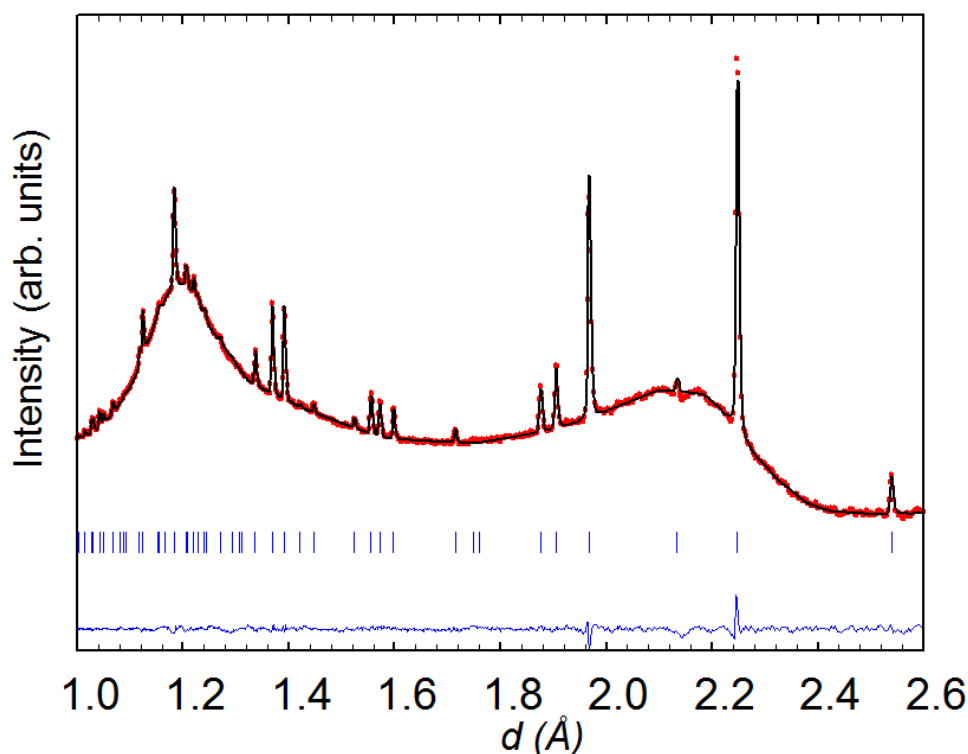


Figure 8. Rietveld refinement (space group $P4/mmm$) from the backscattering detector bank for $\text{NdBaCo}_2\text{O}_{5+\delta}$ at 260 °C in wet (40% D_2O) argon; data collected for 6h.

Table 4. Structural parameters for NdBaCo₂O_{5+δ} (P4/mmm) at 260 °C in 40% D₂O/Ar.

Atom	Position (z) Occupation (Occ.)	$\beta_{11}, \beta_{22}, \beta_{33}$ ($\times 100$)
Nd		2.3(1), 2.3(1), 0.54(5)
Ba		2.0(2), 2.0(2), 0.45(7)
Co	z: 0.2468(7)	1.9(2), 1.9(2), 0.51(7)
O1	Occ: 0.264(8)	[#] 1.72(4)
O2		[#] 1.72(4)
O3	z: 0.2035(2) Occ: 0.944(8)	[#] 1.72(4)
O-content	5.04(4)	

Space group *P4/mmm*, $a = 3.9349(1)$ Å, $c = 7.6197(3)$ Å with sites Nd *1a* (0 0 0), Ba *1b* (0 0 0.5), Co *2h* (0.5 0.5 *z*), O1 *1c* (0.5 0.5 0), O2 *1d* (0.5 0.5 0.5), O3 *4i* (0.5 0 *z*), [#] B_{iso} constrained to be equal, $\chi^2 \sim 2.2$, $R_B \sim 3\%$, $R_F \sim 3.7\%$.

3.3.2 NdBaCo_{1.5}Mn_{0.5}O_{5+δ}

The thermal evolution of the Mn-substituted composition ($x = 0.5$) in dry argon is very similar to that of the pure cobalt material ($x = 0$), except that there is no orthorhombic \rightarrow tetragonal phase transition as the Mn-compound is already tetragonal. The temperature dependence of the oxygen stoichiometry, determined from the Rietveld analysis of the data listed in Table 5 indicates that the oxygen content remains close to 5.0/f.u.. These results show that there is no influence of the oxygen content, particularly a large oxygen deficiency on the reactivity of the NdBaCo_{2-x}Mn_xO_{5+δ} ($x = 0, 0.5$) compounds with water (i.e. water dissociation) in wet argon. Conversely, in Ruddlesden-Popper compounds such as Sr₃Fe₂O_{7-δ} and PrSr₃Co_{1.5}Fe_{1.5}O_{10-δ}, the oxygen stoichiometry (δ) considerably influences hydration properties^{27, 32-33}.

Table 5. Oxygen occupancy of $\text{NdBaCo}_{1.5}\text{Mn}_{0.5}\text{O}_{5+\delta}$ determined from neutron diffraction data in wet argon. The occupancy factor for O2 was fixed at 1.0. Collection time is indicated in parenthesis.

T (°C)	800 (30 min)	260 (14h)	300 (5h)	400 (3h)	500 (2h)	260 (11h)	200 (20min)
Atom							
O1	0.072(8)	0.072(0)	0.080(8)	0.072(8)	0.064(8)	0.080(8)	0.064(8)
O3	0.95(4)	0.98(1)	0.99(2)	0.97(2)	0.96(2)	0.99(2)	0.97(3)
O-content/f.u.	4.9(2)	4.98(5)	5.03(7)	4.94(7)	4.90(8)	5.03(7)	5.0(1)

Refinement with anisotropic ADPs for all the atoms except B_{iso} for (Co,Mn) and $B_{iso} = 0$ for O1.

Figure 9 displays the Rietveld refinement of the data collected for 11 h at 260 °C in wet argon with Table 6 listing the corresponding structural parameters.

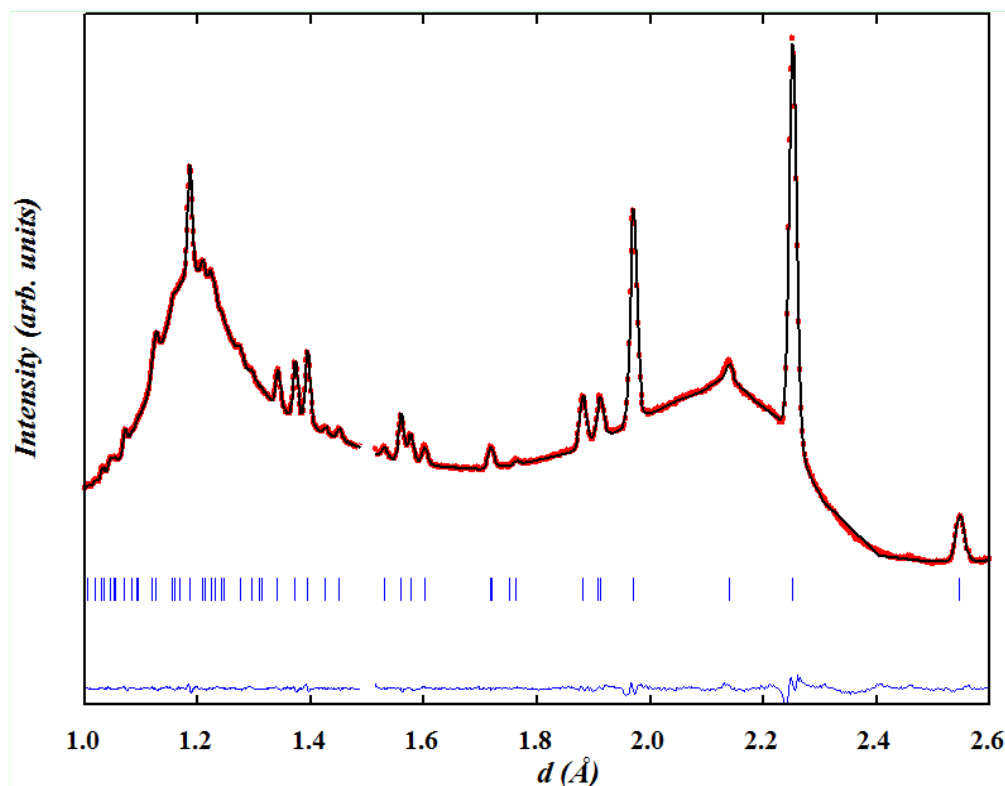


Figure 9. Rietveld profile (bank 5) for $\text{NdBaCo}_{1.5}\text{Mn}_{0.5}\text{O}_{5+\delta}$ in wet argon at 260 °C; data collected for 11 h. Refinement with anisotropic ADPs for all the atoms except for (Co,Mn) for which B_{iso} was refined and B_{iso} for O1 fixed at 0.

Table 6. Structural parameters for NdBaCo_{0.5}Mn_{0.5}O_{5+δ} (S.G. *P4/mmm*) at 260 °C in 40% D₂O/Ar.

Atom	Position (z) Occupancy (Occ.)	$\beta_{11}, \beta_{22}, \beta_{33}$ ($\times 100$)
Nd		1.9(1), 1.9(2), 0.28(5)
Ba		1.7(2), 1.7(2), 0.7(1)
Co,Mn	z: 0.252 (2)	*0.7(2)
O1	Occ: 0.080(8)	[#] $B_{\text{iso}} = 0$
O2		2.3(2), 2.3(2), 0.32(7)
O3	z: 0.1986 (2) Occ: 0.99(2)	2.0(2), 2.6(2), 0.81(5)
O-content	5.03(7)	

*Refined isotropically, [#]fixed.

The behaviour of the $x = 0.5$ sample in dry and wet argon is governed by thermal expansion and exhibits some hysteresis at low temperature (e.g. at 260 °C) likely due to low equilibration. The evolution of the structural parameters is displayed in Figure S.I. 3.

3.4 Structural evolution in wet air

3.4.1 NdBaCo₂O_{5+δ}

As soon as the gas was changed from wet argon to wet air at 260 °C, the single-phase model no longer gave a satisfactory fit to the data collected on the $x = 0$ sample. The presence of extra peaks clearly evidenced the growth of a second phase. Figure 10 shows the data sets collected in the temperature range 260 - 800 °C. The changes were mainly observed in the (200) Bragg peak (index corresponding to *P4/mmm* symmetry) which is almost the only reflection available to study the evolution of the initial phase and the new one. The other peaks overlap due to the similarity in the structures and compositions of the two phases.

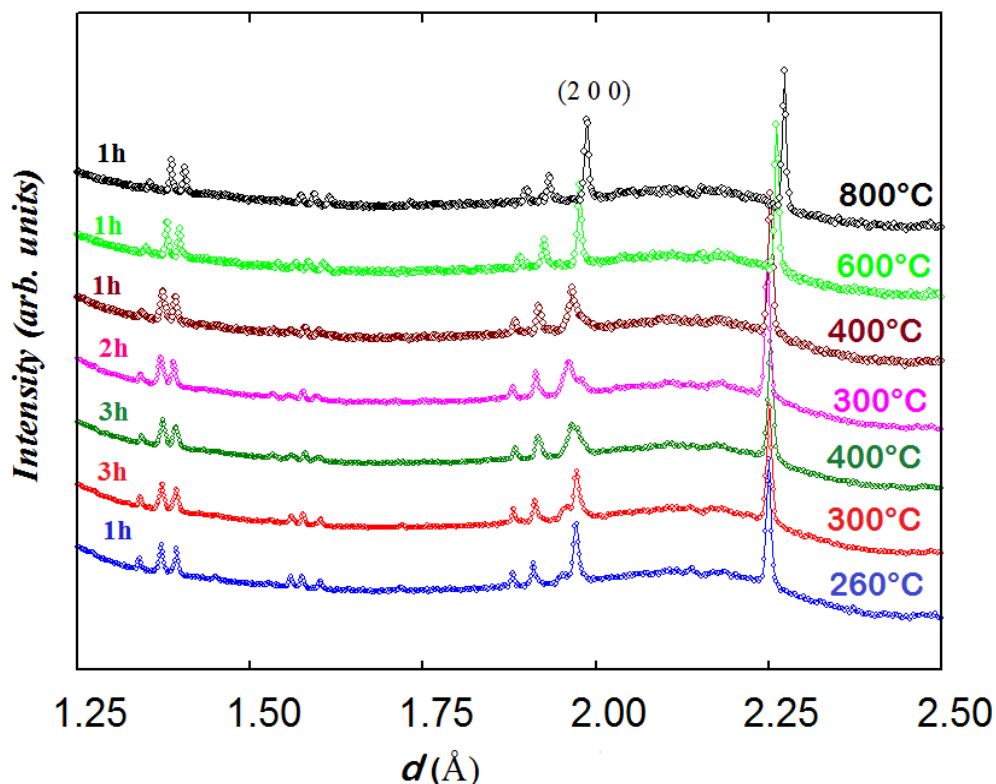


Figure 10. Evolution of the NPD patterns (bank 5) of $\text{NdBaCo}_2\text{O}_{5+\delta}$ obtained in wet air from 260 to 800 °C, index corresponds to $P4/mmm$ symmetry. The two orthorhombic phases co-exist in the temperature range 260–400 °C; the collection duration of each data set is indicated; time increases upwards.

The data collected at 260 °C for 1 h, were initially fitted with two tetragonal phases with different lattice parameters and oxygen content; however the model did not resemble the observed pattern well with the reliability factors; global $\chi^2 \sim 1.45$, $R_B \sim 8.0\%$, $R_F \sim 5.6\%$ for phase 1 and $R_B \sim 3.0\%$, $R_F \sim 4.6\%$ for phase 2. Use of two orthorhombic phases yielded lower reliability factors; global $\chi^2 \sim 1.0$, $R_B \sim 5.7\%$, $R_F \sim 4.8\%$ for phase 1 and $R_B \sim 3.0\%$, $R_F \sim 4.4\%$ for phase 2. It is interesting to mention that using a single orthorhombic phase resulted in a higher reliability factor $\chi^2 = 1.8$.

In contrast to the ordered vacancies $Pmmm$ structural model ($a_p \times 2a_p \times 2a_p$) which fits the data of the as-prepared material at RT and on heating in dry Ar up to 400 °C, an orthorhombic model $Pmmm$ ($a_p \times a_p \times 2a_p$) that assumes disordered vacancies and consists of a single Co site and four different oxygen sites O1, O2, O3 and O4 was used in the two-phase refinements due to the large number of parameters and similarity of the two phases. All the sites were refined with isotropic ADP. Due to the low occupancy at the O1 site in the Nd layer and similar symmetry with the O2 site in the Ba layer, B_{iso} for

O1 and O2 were constrained to be identical. Due to strong correlations between B_{iso} and site occupancy for O3 and O4 (which are localized at the equatorial positions of the Co polyhedra and accommodate very little oxygen vacancies), B_{iso} , occupancy and z positions of O3 and O4 were constrained to be the same in each phase. Relaxing these constraints did not change the quality of the refinement. Refinement of two strain broadening parameters; S_{400} and S_{040} were needed to fit accurately the data collected during the intercalation process and must be constrained to be equal for the two banks and the two phases to allow sensible evolution of the weight ratios as a function of time. The O3/O4 sites in phase 2 (oxidised phase) were found to be fully occupied and their occupancy was fixed at 1.0 in all of the two-phase refinements. Oxygen vacancies were mainly localised at the O1 site in the two phases although lesser in phase 2 than in phase 1 and very little vacancy content was found at the O3/O4 sites of phase 2. The distortion of the basal plane of the intercalated phase (phase 2) at 260 °C ($a = 3.94483(7)$, $b = 3.8960(8)$ Å) whose oxygen content refined to 5.5(2) atoms/f.u. is more pronounced than in the initial phase 1 ($a = 3.9345(8)$, $b = 3.9315(9)$ Å) whose oxygen-content refined to 4.9(1) atoms/f.u. In addition, the c parameter of phase 2 is larger than in phase 1; 7.633(2) vs 7.6181(6) Å, in agreement with larger oxygen content (or proton defects) in the former. The fit of the pattern collected for 1h at 260 °C in wet air is displayed in Figure 11.

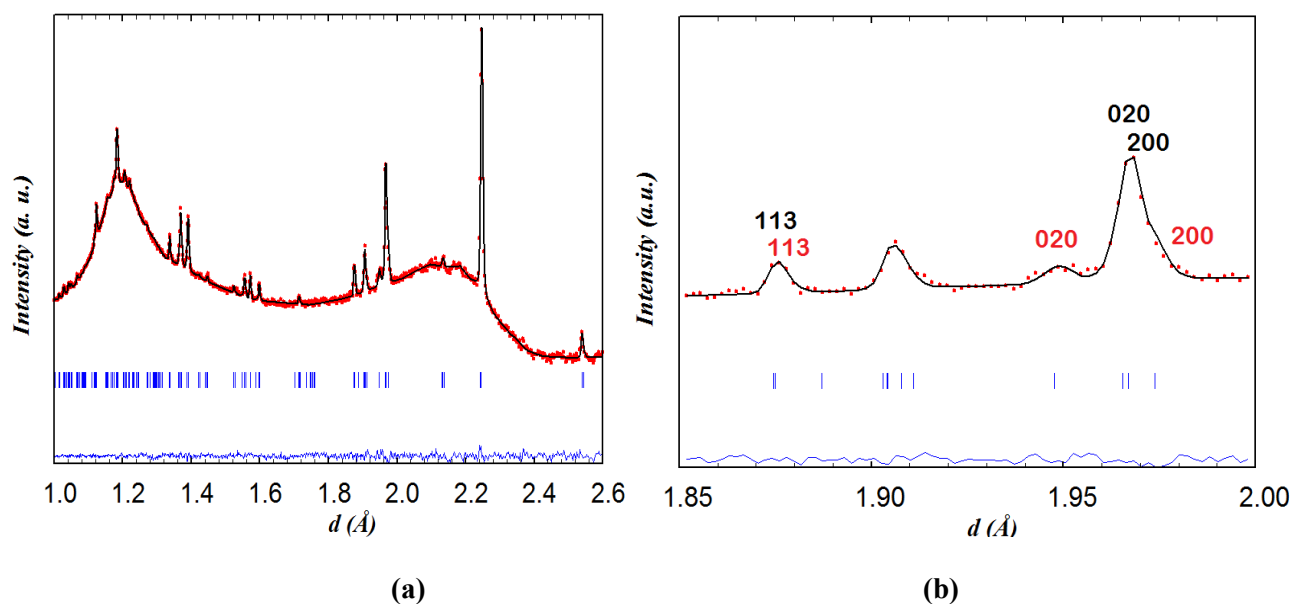


Figure 11. (a) Two-phase fit (bank 4) of neutron diffraction data collected on $\text{NdBaCo}_2\text{O}_{5+\delta}$ for 1h at 260 °C in wet air, (b) contributions of (black) phase 1 and (red) phase 2.

Heating above 260 °C, enhances the nucleation and growth of the second phase whose δ value remains almost constant, at $\sim 0.5(2)$ in the temperature range 260-400 °C. The oxygen content of phase 1 increases with time although it remains lower than that of phase 2 as illustrated in Fig. 12c. After 7 hours of heating in wet air, the two phases have a similar weight ratio and an “inversion” of the orthorhombicity is produced: the a and b lattice parameters of phase 2 which were significantly different at 260 °C become similar at 400 °C ($a = 3.929(4)$, $b = 3.921(4)$ Å) whereas phase 1 which was pseudo tetragonal at 260 °C ($a = 3.9345(8)$, $b = 3.9315(9)$ Å) becomes significantly orthorhombic at 400 °C ($a = 3.949(1)$, $b = 3.9134(9)$ Å) as shown in Fig. 12a. This behavior may be due to increased oxygen content in both phases (Fig. 12c) and possible ordering of the oxygen vacancies in phase 1 whose δ value approaches 0.5. The evolution of the c lattice parameters is mainly governed by thermal expansion (Fig. 12b) rather than chemical expansion consecutive to variations in the oxygen content and show the presence of some hysteresis (e.g. at 400 °C). The c lattice parameter of phase 2 remains larger than that of phase 1 in agreement with larger oxygen content in the former. Heating at 600 °C promotes the intercalation reaction kinetically and the two phases merge into a single tetragonal phase with $\delta \sim 0.4(2)$ oxygen atoms/f.u. suggesting that the oxygen transport at 600 °C is sufficiently rapid to overcome the kinetic limitations experienced at lower temperatures. The sample remains single tetragonal phase at 800 °C and on subsequent cooling. No secondary phases were detected at any temperature. In the temperature range of coexistence of the two phases, the sample undergoes a fast intercalation reaction between an oxygen deficient ($\delta \sim 0$) and an oxygen rich phase ($\delta \sim 0.5(2)$). Variation of the cell parameters, oxygen content and weight fractions are displayed in Figure 12.

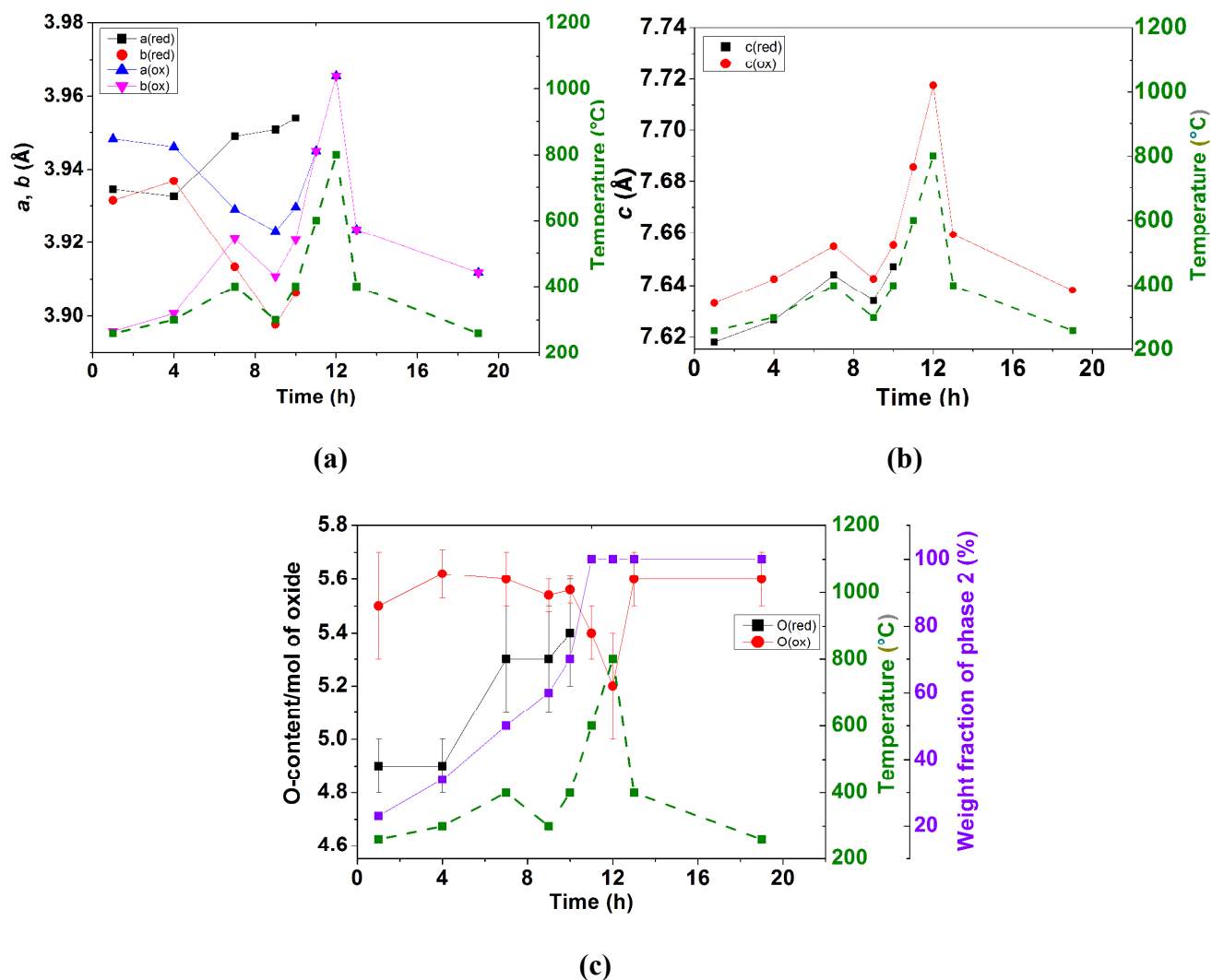


Figure 12. Structural variation for NdBaCo₂O_{5+δ} ($x = 0$) in wet air; (a) a and b lattice parameters, (b) c lattice parameter (d) oxygen content and weight fraction of phase 2.

3.4.2 NdBaCo_{1.5}Mn_{0.5}O_{5+δ}

The behavior of the $x = 0.5$ composition in wet air is similar to that of the $x = 0$ phase and indicates the growth of an intercalated oxidised phase. Only two data sets were collected in wet air on this composition; at 200 and 300 °C. In contrast to the two-phase orthorhombic model used to fit the data collected on the $x = 0$ composition, a two-phase tetragonal model was used to fit these data. The reliability factors χ^2 for the two-phase model are 2.6 and 2.1 at 200 and 300 °C respectively in comparison to $\chi^2 = 4.9$ and 3.9 when a single tetragonal phase is used.

The two-phase tetragonal model consistent with the diffraction pattern recorded at 200 and 300 °C for 90 minutes is shown in Figure 13. The main results of the Rietveld refinements are displayed in Table 7. At 200 °C, the smaller a - and larger c - lattice parameters of phase 2 (oxidised phase) with respect to phase 1 (reduced phase) are consistent with larger oxygen content in the former. This behaviour is exhausted at 300 °C where the proportion of phase 2 has reached $\sim 80\%$.

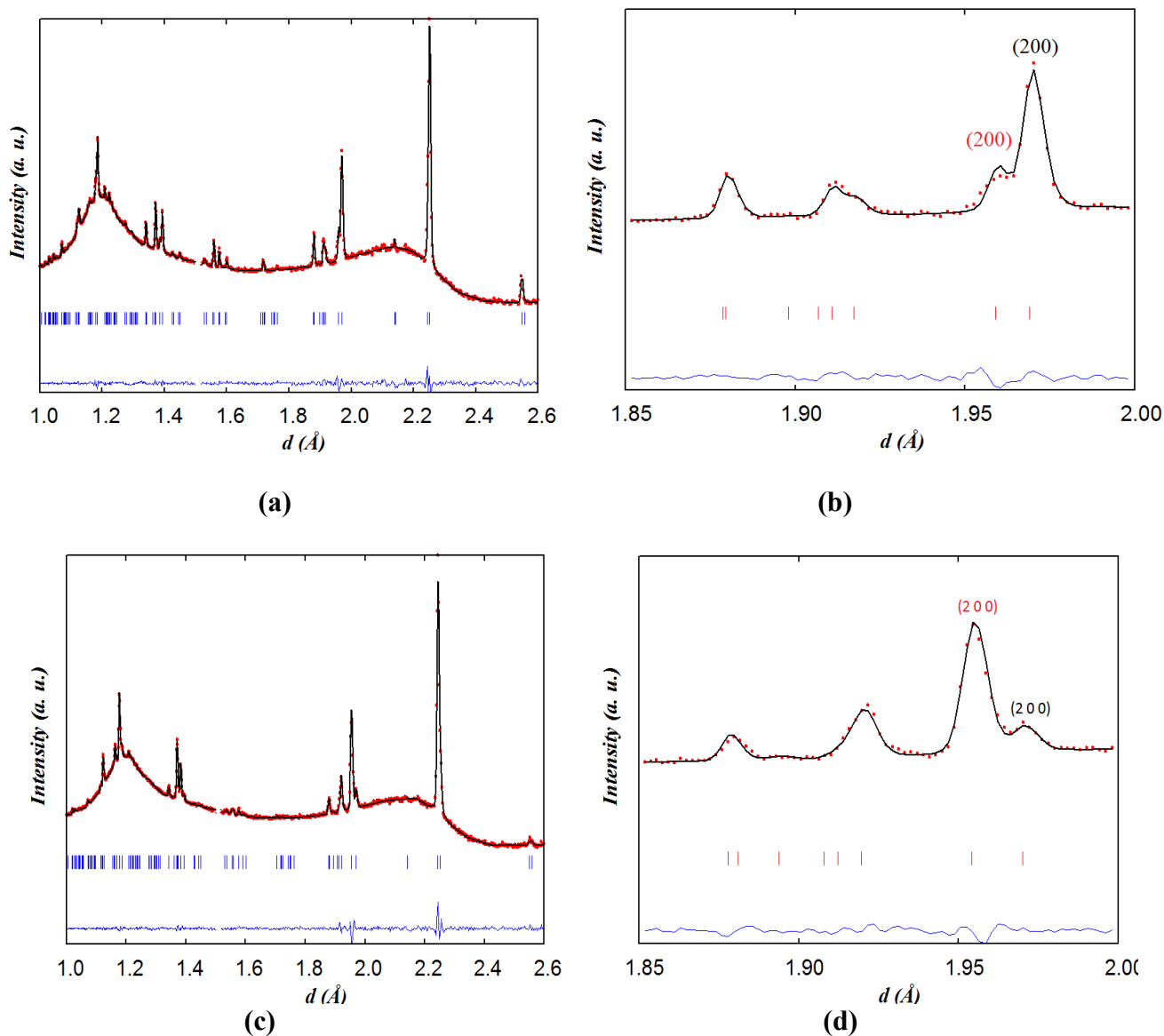


Figure 13. Two-phase fits for neutron data collected on $\text{NdBaCo}_{0.5}\text{Mn}_{0.5}\text{O}_{5+\delta}$ in wet air for 90 minutes at (a, b) 200 °C and (c,d) 300 °C using a tetragonal model; (red) intercalated and (black) reduced phases.

Table 7. Main results of the Rietveld refinements in $P4/mmm$ for $\text{NdBaCo}_{1.5}\text{Mn}_{0.5}\text{O}_{5+\delta}$ in wet air

	Phase 1	Phase 2
200°C (1h30)		
$a(\text{Å})$	3.9380 (2)	3.9179 (4)
$c(\text{Å})$	7.6421 (5)	7.6685 (2)
Occ. O1	0.056 (8)	0.40 (6)
Oxygen content	5.12(2)	5.8 (1)
Weight fraction (%)	80	20
300 °C (1h30)		
$a(\text{Å})$	3.9405 (5)	3.9090 (2)
$c(\text{Å})$	7.653 (2)	7.6809 (5)
Occ. O1	0.17 (4)	0.42 (2)
Oxygen content	5.33 (8)	5.82 (3)
Weight fraction (%)	20	80

The occupation of O3 has been fixed at 1.0.

The reason for the existence of the two phases during exposure of the $x = 0$ and 0.5 samples to wet air may stem from the two accessible values of δ for the $\text{NdBaCo}_2\text{O}_{5+\delta}$ and $\text{NdBaCo}_{1.5}\text{Mn}_{0.5}\text{O}_{5+\delta}$ compositions, close to 0.0 and 0.5 with a portion of the sample oxidizing preferentially. The need for two phases to fit the data collected in wet air for 10 h up to 400 °C on the $x = 0$ sample may indicate that the kinetics of oxidation are relatively slow and that the oxidation process is limited for the time that the samples were held at each temperature between 260 and 400 °C (1-3 hours) because of the low flow rate of the gas (20 mL min⁻¹) and the large quantity of the powder sample used in the neutron experiment (~ 4 g). Conversely, the TGA experiment, using a smaller quantity of sample (100 mg) and higher flow rate (10 mL min⁻¹) would suggest that the surface exchange and diffusion of oxygen are fast in the reduced phase under these conditions.

Although our diffraction experiment highlighted the stability of the layered phases $x = 0$ and 0.5 in humid conditions, it was difficult to establish the incorporation of proton defects in this oxides family. Water dissociation strongly depends on the basicity of the ceramics and the presence of the Ba cation at the A site. This basicity is however lowered by the substitutions with less basic elements such as Nd which prevents the reaction with acidic gases such as H₂O and therefore hydrolysis. It is worthwhile stressing that despite intensive studies on systems that insert a large amount of proton defects such as

the brownmillerite $\text{Ba}_2\text{In}_2\text{O}_5$ and derived compositions³⁴⁻³⁵ and orthorhombic perovskite $\text{BaCe}_{0.9}\text{Y}_{0.1}\text{O}_{2.95}$ ³⁶ or cubic $\text{La}_{0.73}\text{Ba}_{0.27}\text{ScO}_{2.865}$ ³⁷ or $\text{SrZr}_{0.95}\text{Sc}_{0.05}\text{O}_{3-\delta}$ ³⁸ perovskites, the determination of the proton site is only suggested at very low temperatures, far from the conducting conditions. It should be mentioned that the improvement of the electrochemical properties of the layered cobaltite $\text{PrBaCo}_2\text{O}_{5+\delta}$ with increased $p\text{H}_2\text{O}$ reported by Grimaud *et al.*¹³ can be related to the formation of secondary phases such as hydroxides which are very good proton conductor and consequently did not reflect the properties of their materials. Indeed, Jalarvo *et al.*³⁹ showed by *in situ* synchrotron X-ray diffraction that in the case of the proton conducting perovskites, $\text{Sr}_4(\text{Sr}_2\text{Nb}_2)\text{O}_{11.n}\text{H}_2\text{O}$ and $\text{Sr}_4(\text{Sr}_2\text{Ta}_2)\text{O}_{11.n}\text{H}_2\text{O}$, secondary phases such as $\text{Sr}(\text{OH})_2$ can dominate proton conduction.

Conclusion

The vacancy ordered $\text{NdBaCo}_{2-x}\text{Mn}_x\text{O}_{5+\delta}$ ($x = 0, 0.5$) layered perovskites have been investigated in dry and wet argon and wet air by *in situ* high temperature neutron powder diffraction. The materials were found to be stable in strongly humid conditions up to 800 °C. However the incorporation of proton defects could not be clearly established from our *in situ* data collected in wet conditions at high temperature. This suggests that the basic character of the $\text{NdBaCo}_{2-x}\text{Mn}_x\text{O}_{5+\delta}$ phases owing to the Ba cation along with the presence of large amount of oxygen deficiency and high oxygen mobility which are the key factors involved in the mechanism of water dissociation/insertion in cubic perovskite proton conducting electrolytes (e.g. acceptor-doped doped barium zirconates and cerates) appear not to be the most relevant factors for water dissociation/incorporation in the ordered Co-based double perovskites studied.

Acknowledgments

One of the authors (M. B.) thanks P. D. Battle (Oxford University) and T. Roisnel (University of Rennes) for much helpful advice during the course of the refinements as well as G. Gauthier (Industrial University of Santander) who provided with very valuable comments. The authors also thank R.

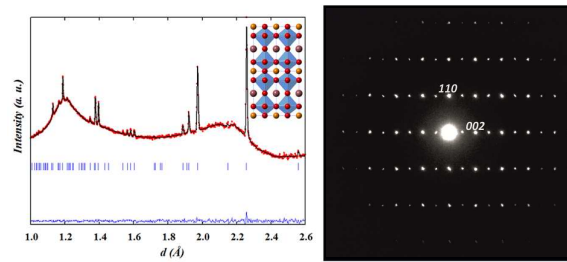
Haynes and the rest of sample environment team at ISIS for their assistance. This research was partially supported by the ANR IDEA-MAT grant (ANR-A2-BS08-0012-01) which provided a Post-doctoral Fellowship for J. Hanlon.

References

1. D. J. L. Brett, A. Atkinson, N. P. Brandon and S. J. Skinner, *Chemical Society Reviews*, 2008, 37, 1568-1578.
2. S. C. Singhal and K. Kendall, *High Temperature Solid Oxide Fuel Cells: Fundamentals, Design and Applications*, Oxford, 2003.
3. B. C. H. Steele and A. Heinzl, *Nature*, 2001, 414, 345-352.
4. C. Zuo, S. Zha, M. Liu, M. Hatano and M. Uchiyama, *Advanced Materials*, 2006, 18, 3318-3320.
5. H. Iwahara, *Solid State Ionics*, 1996, 86-88, Part 1, 9-15.
6. H. Iwahara, T. Yajima, T. Hibino and H. Ushida, *Journal of The Electrochemical Society*, 1993, 140, 1687-1691.
7. K. D. Kreuer, *Annual Review of Materials Research*, 2003, 33, 333-359.
8. K. D. Kreuer, *Solid State Ionics*, 1997, 97, 1-15.
9. T. Norby, *Solid State Ionics*, 1999, 125, 1-11.
10. B. Lin, S. Zhang, L. Zhang, L. Bi, H. Ding, X. Liu, J. Gao and G. Meng, *Journal of Power Sources*, 2008, 177, 330-333.
11. H. Uchida, S. Tanaka and H. Iwahara, *J Appl Electrochem*, 1985, 15, 93-97.
12. G. Goupil, T. Delahaye, B. Sala, F. Lefebvre Joud and G. Gauthier, *Solid State Ionics*, 2014, 263, 15-22.
13. A. Grimaud, F. Mauvy, J. M. Bassat, S. Fourcade, L. Rocheron, M. Marrony and J. C. Grenier, *Journal of The Electrochemical Society*, 2012, 159, B683-B694.
14. A. Maignan, C. Martin, D. Pelloquin, N. Nguyen and B. Raveau, *Journal of Solid State Chemistry*, 1999, 142, 247-260.
15. A. Tarancon, S. J. Skinner, R. J. Chater, F. Hernandez-Ramirez and J. A. Kilner, *Journal of Materials Chemistry*, 2007, 17, 3175-3181.
16. A. Tarancón, A. Morata, G. Dezanneau, S. J. Skinner, J. A. Kilner, S. Estradé, F. Hernández-Ramírez, F. Peiró and J. R. Morante, *Journal of Power Sources*, 2007, 174, 255-263.
17. K. V. Kordesch and G. R. Simader, *Chemical Reviews*, 1995, 95, 191-207.
18. T. Broux, M. Bahout, J. M. Hanlon, O. Hernandez, S. Paofai, A. Berenov and S. J. Skinner, *Journal of Materials Chemistry A*, 2014, 2, 17015-17023.
19. V. F. Sears, *Neutron News*, 1992, 3.
20. Mantid, *Manipulation and Analysis Toolkit for Instrument Data. Mantid Project*, 2013.
21. J. Rodríguez-Carvajal, *Physica B: Condensed Matter*, 1993, 192, 55-69.
22. P. W. Stephens, *Journal of Applied Crystallography*, 1999, 32, 281-289.
23. K. D. Kreuer, *Solid State Ionics*, 1999, 125, 285-302.
24. A. S. Nowick and Y. Du, *Solid State Ionics*, 1995, 77, 137-146.
25. S. Streule, A. Podlesnyak, E. Pomjakushina, K. Conder, D. Sheptyakov, M. Medarde and J. Mesot, *Physica B: Condensed Matter*, 2006, 378-380, 539-540.

26. J. C. Burley, J. F. Mitchell, S. Short, D. Miller and Y. Tang, *Journal of Solid State Chemistry*, 2003, 170, 339-350.
27. M. Lehtimäki, H. Yamauchi and M. Karppinen, *Journal of Solid State Chemistry*, 2013, 204, 95-101.
28. J. H. Kim, L. Moggi, F. Prado, A. Caneiro, J. A. Alonso and A. Manthiram, *Journal of the Electrochemical Society*, 2009, 156, B1376-B1382.
29. R. A. Cox-Galhotra, A. Huq, J. P. Hodges, J.-H. Kim, C. Yu, X. Wang, A. J. Jacobson and S. McIntosh, *Journal of Materials Chemistry A*, 2013, 1, 3091-3100.
30. I. Sosnowska, R. Przeniosło, W. Schäfer, W. Kockelmann, R. Hempelmann and K. Wysocki, *Journal of Alloys and Compounds*, 2001, 328, 226-230.
31. T. Shimoyama, T. Tojo, H. Kawaji, T. Atake, N. Igawa and Y. Ishii, *Solid State Ionics*, 2008, 179, 231-235.
32. L. Jantsky, H. Okamoto, A. Demont and H. Fjellvåg, *Inorganic Chemistry*, 2012, 51, 9181-9191.
33. M. Matvejeff, M. Lehtimäki, A. Hirasa, Y. H. Huang, H. Yamauchi and M. Karppinen, *Chemistry of Materials*, 2005, 17, 2775-2779.
34. V. Jayaraman, A. Magrez, M. Caldes, O. Joubert, F. Taulelle, J. Rodriguez-Carvajal, Y. Piffard and L. Brohan, *Solid State Ionics*, 2004, 170, 25-32.
35. I. Ahmed, C. S. Knee, M. Karlsson, S. G. Eriksson, P. F. Henry, A. Matic, D. Engberg and L. Börjesson, *Journal of Alloys and Compounds*, 2008, 450, 103-110.
36. K. S. Knight, *Solid State Ionics*, 2001, 145, 275-294.
37. E. Kendrick, K. S. Knight, M. S. Islam and P. R. Slater, *Solid State Ionics*, 2007, 178, 943-949.
38. T. Ito, T. Nagasaki, K. Iwasaki, M. Yoshino, T. Matsui, N. Igawa and Y. Ishii, *Solid State Ionics*, 2006, 177, 2353-2356.
39. N. Jalarvo, C. Haavik, C. Kongshaug, P. Norby and T. Norby, *Solid State Ionics*, 2009, 180, 1151-1156.

TOC_ID TA-ART-04-2015-002776



NdBaCo₂O_{5+δ} Rietveld fit at 600°C in wet air and SAED at *RT* along $[1\bar{1}0]$ after 40h heating in wet atmosphere.